PROCEEDINGS OF SCIENCE

Constraints on High Energy Neutrino density from Large Scale Structure

Alberto Gálvez Ureña,[a,*] **Federico Urban**[a] **and David Alonso**[b]

[a] *CEICO—FZU, Institute of Physics of the Czech Academy of Sciences, Na Slovance 1999/2, 182 00 Prague, Czech Republic*

[b] *Department of Physics, University of Oxford, Denys Wilkinson Building, Keble Road, Oxford OX1 3RH, United Kingdom*

E-mail: urena@fzu.cz

Despite growing statistics, the sources of high energy neutrinos remain unknown. Direct source association and stacking analysis have only been able to account for a small fraction of the astrophysical neutrino flux. Here we present an approach that builds on previous work [1, 2] to this problem that makes use of the angular, harmonic cross-correlation between IceCube data and galaxy surveys. If neutrino sources follow the Large Scale Structure (LSS), this cross-correlation should be non zero. If detected, we could learn about how neutrino sources correlate with the LSS via the linear bias and calculate the neutrino emissivity. In this proceedings we show the method to do this while focusing on constraining physical parameters. In the future this information could be used to exclude certain neutrino source models.

39th International Cosmic Ray Conference (ICRC 2025)
15–24 July 2025
Geneva, Switzerland

*Speaker

ISSN 1824-8039. Published by SISSA Medialab.

PoS(ICRC2025)1052

1. Introduction

Determining the sources of high energy neutrinos, first detected by IceCube, remains an open problem. Some source association has been possible, but these only account for a small fraction of the astrophysical neutrino flux. Furthermore, it seems like only around $\sim 10\%$ of astrophysical neutrinos come from the galactic plane [3], thereby the bulk of the sources must be of extragalactic origin.

Extragalactic sources should follow the LSS, which is anisotropic. Therefore, the neutrino distribution will have an imprint of this anisotropy. We try to detect this anisotropy by means of the angular cross-correlation of neutrinos with galaxies. This kind of analysis has proven a powerful tool for other astrophysical messengers as gamma rays [4], ultra-high-energy cosmic rays [5] or gravitational waves [6]. The cross-correlation allows us to measure properties of the underlying neutrino distribution even when individual sources are to weak to be detected.

In this work we present a cross-correlation analysis with emphasis on recovering the physical properties of the neutrino source distribution and its linear bias towards the LSS. For this we use the 10-year IceCube dataset and 4 broad galaxy catalogues: the 2MASS Photometric Redshift catalogue (2MPZ [7]), the WISExSuperCOSMOS catalogue (WIxSC [8]), a sample from the DESI Legacy Imaging Surveys (DECaLS [9]), and the Gaia-unWISE quasar catalogue (Quaia [10]). Together, these catalogues collectively cover the redshift interval $0 < z < 5$. We then interpret our results in terms of two source models and in a model-independent way by taking advantage of our tomographic approach. Our analysis builds upon the cross-correlation studies of [1, 2], but differs in that we focus on the physical parameters that define the absolute neutrino flux by keeping a direct relation between the neutrino redshift distribution and the cross-correlation.

2. Dataset

2.1 Galaxy Catalogues

We use 4 different galaxy catalogues in order to cover a broad redshift range. We select them in such a way that, because of their non-overlapping redshift coverage, they can be used tomographically. For more details on this approach and the galaxy selection see [11]. In summary:

- From the 2MASS Photometric Redshift catalogue 2MPZ we take a sample of 476,190 galaxies under 0.1 redshift, with an average of 0.064. We employ the mask described in [12] to remove the galactic plane and other regions contaminated by stars or dust.
- To the Wise × SuperCOSMOS: WI×SC catalogue we apply the same corrections as described in [12]. We then take a sample with photometric redshift $0.1 < z < 0.4$ with mean redshift of $z_{av} = 0.23$, which consists of 16,325,449 galaxies.
- The third catalogue is built from the DESI Legacy Imaging Surveys: DECaLS. Specifically, we use the sample selected by [9] and apply their corrections for sky contamination. Our sample has a photometric redshift range of $0.3 < z < 0.8$, with an average of $z_{av} = 0.50$.

- The final catalogue is the Gaia-unWISE quasar catalogue: Quaia. We can build a sky mask as described in [13]. Our selected sample has galaxies with $0.8 < z < 5$, with an $z_{av} = 1.72$, for a total of 1,092,207 quasars.

We present in Figure 1 the redshift distribution of each galaxy catalogue after correcting for the photometric redshifts by matching with spectroscopic catalogues. We can see they cover complementary redshift ranges, allowing us to use the tomographic approach described in section 4.

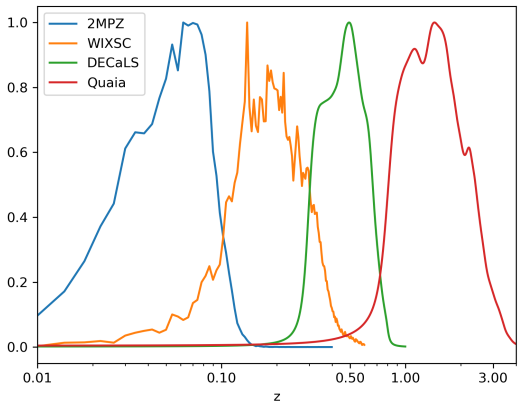

Figure 1: Redshift distribution of the four galaxy catalogues after correcting for the photometric redshifts.

2.2 Neutrino Map

The IceCube 10-year point source dataset is composed from track-like events in which a muon is reconstructed with around 1 degree angular uncertainty. The dataset is composed of 10 seasons with their own observation time, effective area. The effective area is interpolated in a linear manner to have a continuous function of declination and energy $A_{\rm eff}(\delta, \varepsilon_o)$. Then we generate a map for each of the seasons independently, with each event contributing $\frac{1}{A_{\rm eff}}$ to the intensity map. A gaussian beam is also applied to each neutrino according to its angular resolution. Then they are combined to form the total intensity map as

$$\mathcal{I}(\mathbf{n}) = \frac{\sum_{i=1}^{10} \bar{A}^i_{\rm eff}(\mathbf{n})\, \mathcal{I}^i(\mathbf{n})}{\Omega_{\rm pix} \sum_{i=1}^{10} T_i\, \bar{A}^i_{\rm eff}(\mathbf{n})}\,, \tag{1}$$

where $\Omega_{\rm pix}$ it the angular size of each map pixel, T_i is the up-time of season i and $\bar{A}^i_{\rm eff}(\mathbf{n})$ its effective area averaged in energies. This average is done for each pixel p as:

$$\bar{A}^i_{{\rm eff},p} = \frac{1}{\varepsilon^{\alpha+1}_{\rm max} - \varepsilon^{\alpha+1}_{\rm min}} \sum_{n=1}^{N} A_{\rm eff}(\delta_p, \frac{\varepsilon_{n+1} - \varepsilon_n}{2}) \left[\varepsilon^{\alpha+1}_{n+1} - \varepsilon^{\alpha+1}_{n}\right]. \tag{2}$$

Here we have divided the energy range in N bins and averaged them according to a power law with spectral index α. We take $\alpha = -3.7$, according to the tilt of atmospheric neutrinos [14] that compose most of our selected data.

Most of the muons in the data sample are secondary particles from cosmic ray interactions. However, these can be mostly avoided by taking a declination cut of $\delta > -5$. Given the location of IceCube, this cut allows Earth to shield the detector from the atmospheric muons. The second bigger contribution is atmospheric neutrinos, that also are produced as secondary particles of cosmic ray showers. This contribution is unavoidable, but we do know that the fraction of astrophysical neutrinos increases with energy. So we focus on the highest energies, namely $\varepsilon_{\rm min} = 10^3$ GeV to $\varepsilon_{\rm max} = 10^6$ GeV, for a total of 403,529 neutrinos. Furthermore, given that the atmospheric neutrinos have a smooth distribution, we subtract the monopole and dipole from the neutrino map to reduce

the contamination of atmospheric neutrinos on higher multipoles that arises from the non-diagonal covariance matrix due to partial sky coverage. The final neutrino map is shown in Figure 2. All our neutrino and galaxy maps are built with HEALPix [15] as implemented by `healpy` [16].[1]

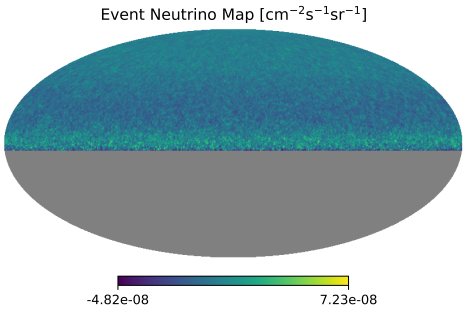

Figure 2: Final neutrino map including beaming and the removal of the monopole and dipole.

In order to compare with our theory model we must take into count the effect of the beaming in the cross-correlation. We follow the method developed in [2]. Briefly, we calculate the effective beam $B_\ell^{\rm eff} \coloneqq \frac{C_\ell^{\bar{\nu}\bar{\nu}}}{C_\ell^{\nu\nu}}$, where $C_\ell^{\bar{\nu}\bar{\nu}}$ is the auto-correlation for the map with the individual Gaussian beams and $C_\ell^{\nu\nu}$ is the same for the neutrino map without any smoothing. We then multiply this by our theory prediction before comparing with the data.

3. Theory

3.1 From neutrino intensity to emissivity

The data represent the neutrino intensity, defined as the number of neutrinos detected per per unit time, energy, detector area, and solid angle in the observers frame

$$I_N \coloneqq \frac{dN_o}{d\varepsilon_o dt_o dA_o d\Omega_o} \,. \tag{3}$$

Considering sources within a range of comoving distances $d\chi$ around χ, we can then relate the intensity to the neutrino emissivity (the number of neutrinos emitted per unit energy, time, and volume in the emitter's frame):

$$dI_N \coloneqq \frac{j_N(\chi\mathbf{n}, z, \varepsilon_e)}{4\pi(1+z)^3} d\chi \coloneqq j_{N,c}(\chi\mathbf{n}, z, \varepsilon_e)\frac{d\chi}{4\pi} \,, \tag{4}$$

Where $j_{N,c}$ is the comoving emissivity and quantities labelled o or e are in the observer or emitter frames respectively. Then, assuming that neutrinos only lose energy due to cosmological redshift, the integrated intensity that we measure is:

$$\mathcal{I}(\mathbf{n}) \coloneqq \int_{\varepsilon_{\rm min}}^{\varepsilon_{\rm max}} d\varepsilon_o \, I(\mathbf{n}, \varepsilon_o) \quad ; \quad I(\mathbf{n}, \varepsilon_o) = \int \frac{d\chi}{4\pi} j_c(\chi\mathbf{n}, z, \varepsilon_o(1+z)) \,. \tag{5}$$

3.2 Modelling the neutrino emissivity

For a simple model we assume that all sources follow a common spectrum $L_\nu \, s(\varepsilon_e)$ such that $\int d\varepsilon_e \, s(\varepsilon_e) = 1$. Then given a comoving luminosity function dn_c/dL_ν we can express the neutrino luminosity as

$$j_c(\mathbf{r}, z, \varepsilon_e) = \frac{s_\nu(\varepsilon_e)}{\varepsilon_e} \int dL_\nu \, L_\nu \frac{dn_c}{dL_\nu}(\mathbf{r}, z, L_\nu) \,, \tag{6}$$

[1] http://healpix.sf.net

where $\mathbf{r} \coloneqq \chi\mathbf{n}$. If we further assume that the energy spectrum is a power law with spectral index β, the intensity is

$$\mathcal{I}(\mathbf{n}) = \int \frac{d\chi}{4\pi} \frac{\dot{n}_\nu(\chi\mathbf{n}, z)}{(1+z)^{1-\beta}} \quad , \tag{7}$$

where $\dot{n}_\nu(\mathbf{r}, z)$ is the comoving neutrino density rate integrated over the energy band

$$\dot{n}_\nu(\mathbf{r}, z) \coloneqq \int_{\varepsilon_{\min}}^{\varepsilon_{\max}} d\varepsilon_o \, j_c(\mathbf{r}, z, \varepsilon_o) = \int_{\varepsilon_{\min}}^{\varepsilon_{\max}} d\varepsilon_o \, \frac{s_\nu(\varepsilon_o)}{\varepsilon_o} \int dL_\nu \, L_\nu \, \frac{dn_c}{dL_\nu}(\mathbf{r}, z, L_\nu)$$

In the linear bias approximation we can relate this quantity with the three-dimensional matter overdensity $\delta(\chi\mathbf{n}, z)$

$$\dot{n}_\nu(\mathbf{r}, z) \coloneqq \dot{\bar{n}}_\nu(z) \, [1 + b_\nu \, \delta(\mathbf{r}, z)], \tag{8}$$

where b_ν is the neutrino bias and $\dot{\bar{n}}_\nu(z)$ is the average comoving neutrino density rate over the sphere.

3.3 Angular Harmonic Cross-Correlation

The 2-dimensional anisotropies of any tracer of LSS over the sky can be expressed as the the projection of three-dimensional matter overdensities $\delta(\chi\mathbf{n}, z)$. In particular for the neutrinos we have

$$\Delta_\nu(\mathbf{n}) \coloneqq \int d\chi \, q_\nu(\chi) \, [b_\nu \bar{\nu}](z) \, \delta(\chi\mathbf{n}, z) \, , \tag{9}$$

where, following the previous subsection, $\bar{\nu}$ is $\dot{\bar{n}}_\nu$ and the neutrino kernel $q_\nu(\chi) \coloneqq [4\pi(1+z)^{1-\beta}]^{-1}$. For the galaxies we similarly can write

$$\Delta_g(\mathbf{n}) \coloneqq \int d\chi \, q_g(\chi) \, b_g \, \delta(\chi\mathbf{n}, z) \, , \tag{10}$$

where the galaxy kernel is $q_g(\chi) \coloneqq H(z) \, \frac{dp}{dz}$, with $H(z)$ being the Hubble parameter and $\frac{dp}{dz}$ the redshift distribution of the galaxy sample. Finally, in the Limber approximation that is valid for broad kernels such as ours [17], we can express the neutrino-galaxy cross-correlation and the galaxy-galaxy auto-correlation as

$$C_\ell^{\mathcal{I}_N \, G} = b_g \; b_\nu \int \frac{d\chi}{\chi^2} q_g(\chi) \frac{\dot{\bar{n}}_\nu(z)}{4\pi(1+z)^{1-\beta}} \, P(k/\chi, z) \, , \tag{11}$$

$$C_\ell^{G \, G} = b_g^2 \int \frac{d\chi}{\chi^2} \, [q_g(\chi)]^2 \, P(k/\chi, z) \, . \tag{12}$$

4. Methodology and Results

In order to compute the correlators and their covariance matrices we use the pseudo-C_ℓ method as implemented in `namaster` [18], that takes into account partial sky coverage for all our datasets. We then obtain the theory spectra as in Equation 12 and Equation 11 with the Core Cosmology Library [19].[2] We assume standard ΛCDM cosmology with parameters $\Omega_c = 0.25$, $\Omega_b = 0.05$, $\Omega_k = 0$, $\sigma_8 = 0.81$, $n_s = 0.96$, $h = 0.67$ and no massive neutrinos. We then compare the data to the theory spectra to get first the galaxy bias and then extract information from the cross-correlation.

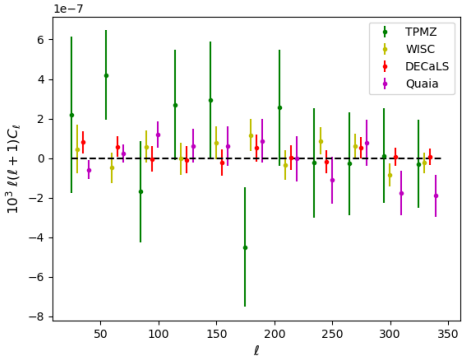

Figure 3: Neutrino-galaxy cross-correlation for all 4 galaxy catalogues.

4.1 Galaxy Bias

We first need to estimate the galaxy bias from the galaxy auto-correlation in order to have one parameter less in Equation 11. This can be done through the likelihood

$$\mathcal{L}(b_g) \coloneqq -\frac{1}{2}\left(\mathbf{C}^D - \mathbf{C}^M(b_g)\right)\mathcal{M}^{-1}\left(\mathbf{C}^D - \mathbf{C}^M(b_g)\right), \tag{13}$$

where $\mathbf{C} \coloneqq C_\ell^{GG}$ (we have suppressed the multipole to avoid clutter). D and M refer to data and model vector, respectively, while $\mathcal{M}$ is the covariance matrix for $\mathbf{C}^D$. For all catalogues we use the linear bias approximation except for Quaia, where we use $b_{\rm Quaia} = b_g * (0.278((1+z)^2 - 6.565) + 2.393)$ [10]. The biases obtained are: 2MPZ: $b_g = 1.212 \pm 0.027$, WixSC: $b_g = 1.1608 \pm 0.0072$, DECaLS: $b_g = 1.4783 \pm 0.0059$, Quaia: $b_g = 1.050 \pm 0.034$.

4.2 Neutrino kernel

The cross-correlation Equation 11 depends on the neutrino source redshift distribution. This is an unknown, so we test two different parametrizations:

$$\dot{\bar{n}}_\nu(z) = N(1+z)^a \quad ; \quad \dot{\bar{n}}_\nu(z) = N(1+z)^2\, e^{-z^2} \tag{14}$$

The first function is a power law with free parameters the normalisation N and the slope α, the second one is fully defined by the normalisation alone and peaks at $z \sim 1$ [2].

4.3 Neutrino-Galaxy Cross-Correlation

Because the contamination due to atmospheric events is more prominent at low multipoles, to minimise its effects we discard all multipoles below $\ell = 10$ and proceed in bins of $\Delta\ell = 30$. We do this up until $\ell_{\rm max} = 340$, since there is no more information after it due to the beaming [2]. Note that

[2] https://github.com/LSSTDESC/CCL

our results are robust against changes in ℓ_{max}. The cross-correlation results are shown in Figure 3. There is no significant detection for the cross-correlation with the individual catalogues.

We can use all the information in the galaxy catalogues in a tomographic fashion by modifying the likelihood as

$$\mathcal{L}(p) \coloneqq -\frac{1}{2}\sum_{G}\left(\mathbf{X}^{D,G} - \mathbf{X}^{M,G}(p)\right)\mathcal{M}^{G^{-1}}\left(\mathbf{X}^{D,G} - \mathbf{X}^{M,G}(p)\right). \tag{15}$$

Here $\mathbf{X} \coloneqq C_\ell^{\mathcal{I}_N\, G}$ and G sums over the galaxy catalogues. The parameters p are either $p \in \{a, Nb_\nu\}$ or $p \in \{Nb_\nu\}$ for the power law and peak models, respectively. For the theory model we take $\beta = 2.5$ following the astrophysical neutrino spectrum measured by IceCube [20]. The parameter estimation is done by the nested sampling Monte Carlo algorithm `MLFriends` [21] as implemented in the `UltraNest` package [22].[3] The prior distributions for the different parameters are: $Nb_\nu \in [-10000, 10000] \cdot 10^{45}\,\mathrm{Mpc}^{-3}\mathrm{yr}^{-1}$ and $a \in [-5, 0]$. We summarise our results in Table 1 and present the allowed regions for $b_\nu \dot{\bar{n}}_\nu$ and their 1σ and 2σ confidence levels in Figure 4.

Model	$Nb_\nu\ \left[10^{45}\,\mathrm{Mpc}^{-3}\,\mathrm{yr}^{-1}\right]$	a
$\dot{\bar{n}}_\nu(z) \propto (1+z)^a$	5.8 ± 3.6	-2.7 ± 1.4
$\dot{\bar{n}}_\nu(z) \propto (1+z)^2\, e^{-z^2}$	4.3 ± 2.4	

Table 1: Best-fit parameters for both source models.

It is also possible to use the tomographic approach to obtain constraints without assuming a specific form for the neutrino kernel. For this we assume that each of our redshift bins are small enough for the neutrino kernel to be approximated by a constant within each bin. We apply the same likelihood Equation 15 but do not sum over galaxy catalogues. The results of this procedure are shown in Table 2 and figure Figure 5.

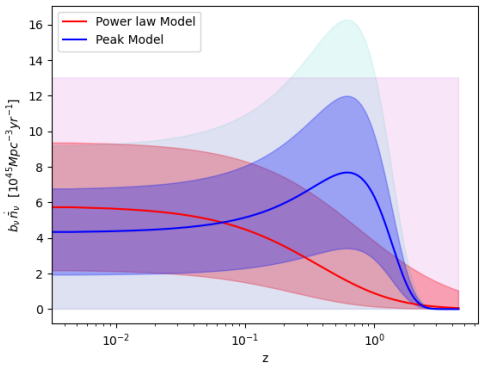

Figure 4: Allowed 1σ and 2σ regions for the density rate of neutrinos times b_ν in the power law and peak models.

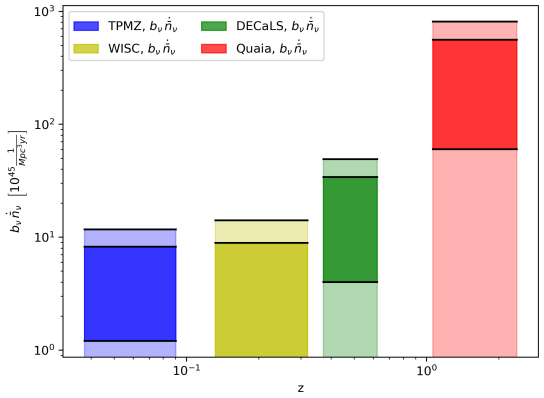

Figure 5: Allowed 1σ and 2σ regions for the number and energy density rates of neutrinos times b_ν in the tomographic approach.

[3] https://johannesbuchner.github.io/UltraNest/

5. Conclusion

In this work we have introduced a new method to use the neutrino-galaxy angular cross-correlation to constrain the physical parameters that define the neutrino sources redshift evolution, together with their clustering properties. In order to do so we used the 10-year point-source IceCube dataset and 4 galaxy catalogues with different redshifts coverage between $0 < z < 5$.

	$b_\nu \dot{\bar{n}}_\nu \left[10^{45}\,\mathrm{Mpc}^{-3}\,\mathrm{yr}^{-1}\right]$
TPMZ	4.7 ± 3.5
WISC	3.7 ± 5.2
DECaLS	19 ± 15
Quaia	310 ± 250

Table 2: Best-fit $b_\nu \dot{\bar{n}}_\nu$ assuming constancy in each redshift bin.

The most significant results are obtained for the peak model, at $\sim 1.8\sigma$ for Nb_ν in the peak model, which is a marginal but nonetheless encouraging positive detection. Future neutrino experiments such as IceCube-Gen2 and KM3NeT, combined with galaxy surveys that will have increased sky coverage and denser sampled redshift distributions, such as the Vera C. Rubin Observatory (LSST) and Euclid are expected to significantly improve the chances for detection of the cross-correlation. Measuring the properties of the redshift evolution of neutrino sources could help us discriminate between different classes of of objects that have been suggested as important contributors of to bulk of the neutrino flux, such as starburst galaxies, tidal disruption events, quasars or Seyfert galaxies.

References

[1] Ke Fang, Arka Banerjee, Eric Charles, and Yuuki Omori. *Astrophys. J.*, 894(2):112, 2020.
[2] Aaron Ouellette and Gilbert Holder. *Phys. Rev. D*, 110(10):103025, 2024.
[3] R. Abbasi et al. *Science*, 380(6652):adc9818, 2023.
[4] Alessandro Cuoco et al. *Astrophys. J. Suppl.*, 221(2):29, 2015.
[5] Federico R. Urban, Stefano Camera, and David Alonso. *Astron. Astrophys.*, 652:A41, 2021.
[6] Alvise Raccanelli et al. *Phys. Rev. D*, 94(2):023516, 2016.
[7] Maciej Bilicki et al. *Astrophys. J. Suppl.*, 210:9, 2014.
[8] M. Bilicki et al. *Astrophys. J. Suppl.*, 225:5, 2016.
[9] Qianjun Hang et al. *Mon. Not. Roy. Astron. Soc.*, 501(1):1481–1498, 2021.
[10] Kate Storey-Fisher et al. *Astrophys. J.*, 964(1):69, 2024.
[11] David Alonso et al. *Phys. Rev. D*, 110(10):103544, 2024.
[12] Nick Koukoufilippas et al. *Mon. Not. Roy. Astron. Soc.*, 491(4):5464–5480, 2020.
[13] David Alonso et al. *JCAP*, 11:043, 2023.
[14] M. G. Aartsen et al. *Eur. Phys. J. C*, 75(3):116, 2015.
[15] K. M. Górski et al. *Astrophys. J.*, 622:759–771, 2005.
[16] Andrea Zonca et al. *Journal of Open Source Software*, 4(35):1298, 2019.
[17] Marilena LoVerde and Niayesh Afshordi. *Phys. Rev. D*, 78:123506, 2008.
[18] David Alonso, Javier Sanchez, and Anže Slosar. *Mon. Not. Roy. Astron. Soc.*, 484(3):4127–4151, 2019.
[19] Nora Elisa Chisari et al. *Astrophys. J. Suppl.*, 242(1):2, 2019.
[20] R. Abbasi et al. *Phys. Rev. D*, 110(2):022001, 2024.
[21] Johannes Buchner. *Statistics and Computing*, 26(1-2):383–392, January 2016.
[22] Johannes Buchner. *The Journal of Open Source Software*, 6(60):3001, April 2021.